

# Anode sheath transition in an anodic arc for synthesis of nanomaterials

V A Nemchinsky<sup>1</sup> and Y Raites<sup>2</sup>

<sup>1</sup> Keiser University, Fort Lauderdale, FL, USA

<sup>2</sup> Princeton Plasma Physics Laboratory, Princeton, NJ, USA

E-mail: [vnemchinsky@keiseruniversity.edu](mailto:vnemchinsky@keiseruniversity.edu) and [yraitse@pppl.gov](mailto:yraitse@pppl.gov)

Received 6 November 2015, revised 22 February 2016

Accepted for publication 10 March 2016

Published 30 March 2016



## Abstract

The arc discharge with ablating anode or so-called anodic arc is widely used for synthesis of nanomaterials, including carbon nanotubes and fullerenes, metal nanoparticles etc. We present the model of this arc, which confirms the existence of the two different modes of the arc operation with two different anode sheath regimes, namely, with negative anode sheath and with positive anode sheath. It was previously suggested that these regimes are associated with two different anode ablating modes—low ablation mode with constant ablation rate and the enhanced ablation mode (Fetterman *et al* 2008 *Carbon* **46** 1322). The transition of the arc operation from low ablation mode to high ablation mode is determined by the current density at the anode. The model can be used to self-consistently determine the distribution of the electric field, electron density and electron temperature in the near-anode region of the arc discharge. Simulations of the carbon arc predict that for low arc ablating modes, the current is driven mainly by the electron diffusion to the anode. For positive anode sheath, the anode voltage is close to the ionization potential of anode material, while for negative anode sheath, the anode voltage is an order of magnitude smaller. It is also shown that the near-anode plasma, is far from the ionization equilibrium.

Keywords: arc, anode, ablation, sheath, nanoparticles

(Some figures may appear in colour only in the online journal)

## 1. Introduction

Since 1991 [1], the carbon arc discharge is widely used for high yield synthesis of carbon nanotubes. In this method, the arc burns between the cathode and the graphite anode. The arc operation is usually maintained at nearly atmospheric pressure helium gas. Under such conditions, the anode is the most thermally loaded electrode in this arc system. Therefore, this electrode ablates due to excessive heating from the plasma. Carbon atoms, molecules and ions are deposited on the cathode forming multi-walled nanotubes, fullerenes and carbon nanoparticles on the cathode surface.

Several important observations have been reported in [2]. First, the copper cathode covered by the carbon deposit is not melted and remained intact during the arc discharge. This observation posed the question about the nature of the electron emission from the cathode [3]. For example, for low ablation rates, it was unclear how the cathode can be heated without

much of ions coming from the anode and forming the deposit on the cathode. Moreover, it was found that the anode ablation rate rises steeply when the anode diameter decreases below a certain level [4]. This increase is usually much larger than could be expected from the increase of the current density at the anode or the reduction of the electrode volume, which is heated up by the arc. This experimental result posed another question of whether the arc operates in two different modes with large and small anodes.

In a recent paper [5], we presented a model of the arc used in carbon arc experiments [2–4]. To address the first question on the source of the cathode heating for a low ablation mode, we suggested a hypothesis of circling the ions trapped in the near-cathode plasma: carbon ion strike the cathode or the cathode deposit formed by carbon ions, atoms and molecules evaporated from the anode, then carbon atoms and molecules evaporate from the cathode deposit and are ionized close to the cathode. The resulting ions are accelerated back to the

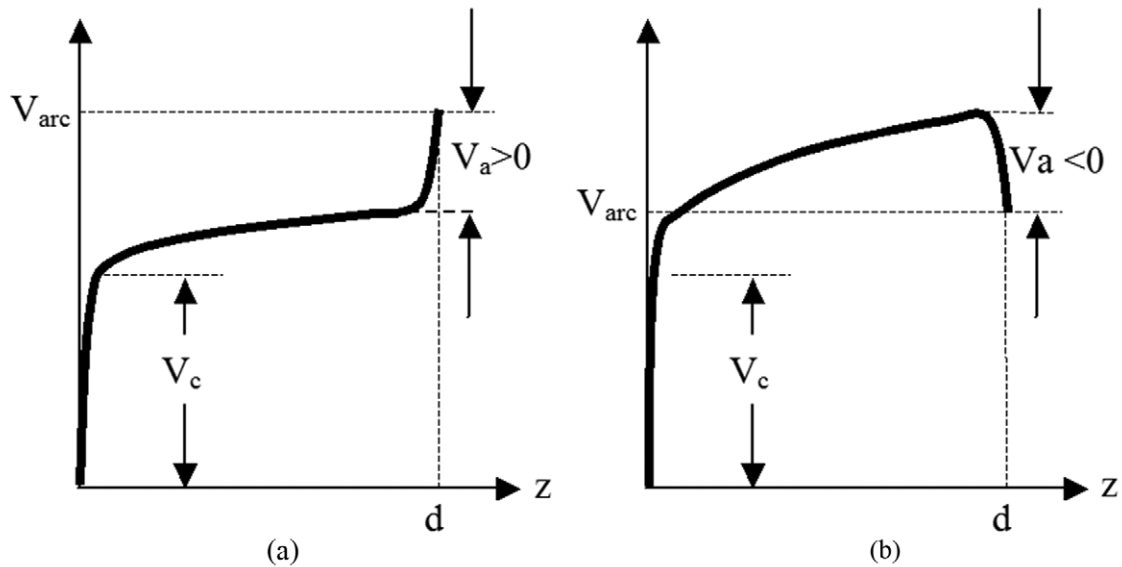


**Figure 1.** Schematic of the potential distribution inside an arc. (a) Positive voltage drop in the anode sheath, negative (electronic) space charge inside the sheath. Ions are reflected from the sheath, electrons are attracted. (b) Negative voltage drop in the anode sheath, positive (ionic) space charge inside the sheath. Ions are pulled inside the sheath, electrons are repelled from it. The total arc voltage  $V_{arc}$  and the cathode voltage drop  $V_c$  are shown.

cathode and so on. This recycling of the carbon atoms and molecules from the cathode deposit allowed us to explain a high current density at the cathode with almost no ion flux from the anode and the plasma column. Moreover, modeling of the thermal processes at the electrodes, and, in particular, at the anode, enabled us to explain the steep rise of the ablation rate by an exponential dependence of the anode evaporation rate on the temperature. However, the existence of different ablation modes was not predicted in our previous work [5]. This is partially because the arc plasma was almost excluded from the model consideration in [5]. As a result, no heat flux to the anode was self-consistently modeled in this work. Instead, we used inputs from experimental data on the arc voltage and some simplified physical considerations and assumptions.

In this paper, we make the next step toward a self-consistent model of the arc with ablating anode. In particular, this paper is focused on the near-anode plasma processes which determine the heat flux to the anode and thereby, the anode ablation rate.

## 2. The anode voltage drop in anodic arcs

A quasi-neutral plasma near the anode is separated from the anode by a non-neutral sheath (figure 1). Space charge in the anode sheath can be either electron attractive with positive anode sheath voltage (so-called positive anode sheath) (figure 1(a)) or electron repelling with negative anode sheath voltage (so-called negative anode sheath) (figure 1(b)).

The sign of the anode sheath in arcs has been a subject to discussions and controversy during the last half of century. In their classical review, Finkenburgh and Maecker [6] analyzing available experiments, considered only the positive anode sheath. They explained the positive anode voltage by the cooling of near-anode plasma by the anode and by decrease in electrical conductivity of the plasma to the anode. The role of

the electron diffusion to the anode, which can force electrons to move even against the electrical field, had not been recognized by that time. Therefore, it was concluded that the electric field should increase toward the anode in order to maintain the current continuity. This conclusion was supported by observations for high current carbon arcs. These arcs operated with strongly evaporating anode in which carbon atoms from the anode swept away the ions moving toward the anode. It was proposed that the friction between atoms and ions should lead to the formation of the positive anode sheath [7].

In mid 70's, the role of the electron diffusion in conduction of the current to the anode was proposed for the first time in [8–10]. It has been shown that electron density declines toward the anode that gives rise to a strong diffusion of electrons to the anode. According to modeling results, this diffusion flow could be comparable to the total electron current or even exceed it. Under such conditions, the electric field can be small or even change polarity to maintain the arc current to the anode. In the latter case, the voltage drop in the anode sheath becomes negative. The reduction of the electric field in the near anode region was later predicted theoretically in [11–13] and obtained in more recent simulations [14, 15].

In arc experiments, electrostatic probes have been used to find potential distribution in the near-anode plasma. [16, 17] reported the reduction of the electric field towards the anode. Experiments by Leveroni and Pfender [18] showed the increase of the electric field near the anode at 60 A arc and the decrease of the electric field at higher currents. In arc experiments by Tanaka and Ushio [19], a qualitatively similar behavior of the electric field was also obtained. A more complete review of relevant experimental results and modeling can be found elsewhere [20, 21]. In short, available experimental data and existing models of the anode region in arc discharges suggest that depending on a particular arc situation, the anode sheath can be either negative or positive. In this

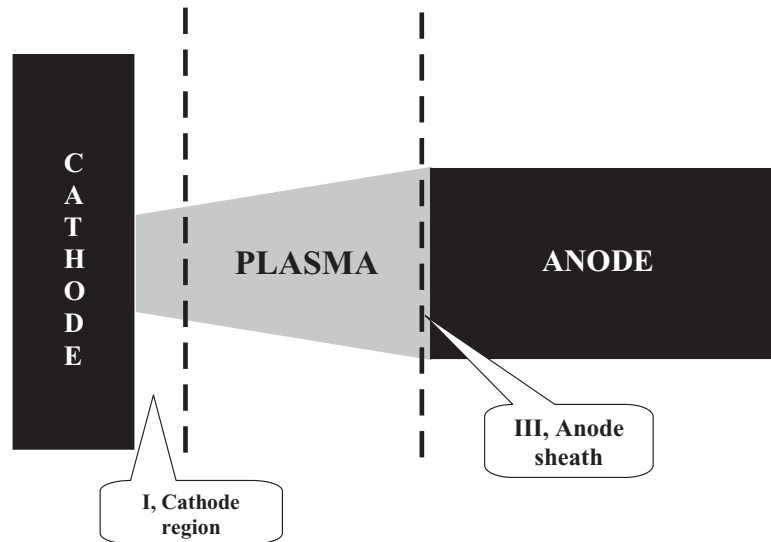


**Figure 2.** Schematic of a typical arc geometry of experiments [2–4].

paper, we present the model of experiments [2–4] that predicts the existence of both anode sheath regimes depending on the anode ablation rate and the anode diameter.

### 3. Anode sheath model

#### 3.1. Existing models of arcs for nanoparticle production

A majority of carbon arc studies is focused on the methods of synthesis of nanoparticles rather than on arc discharge physics. In the existing arc models, much of attention is paid to gas-dynamics of the arc discharge [22–25] rather than to plasma processes. For example, to the best of our knowledge, local thermodynamic equilibrium (LTE) with no justification is commonly assumed in the existing arc models. Diffusion processes, including current conduction, which could be very important for short anodic arcs such as used for nanosynthesis, are not considered for the rare exceptions (e.g. [26]). In different arc modeling studies, different anode sheath regimes were assumed: positive [24, 26], negative [25, 27]. Electron diffusion process was considered only in [26].

#### 3.2. Model formulation. Equations

For convenience of our modeling, we divide the inter-electrode space into three regions, figure 2, including the cathode sheath with the near-cathode plasma (I), plasma column (II) and the anode sheath (III). In [5], we assumed that the size of the arc attachment to the cathode is smaller than the arc attachment to the anode. The increase of the current density at the cathode is necessary to maintain the heating of the arc attachment area at the cathode, which is needed to maintain an electron emission from this electrode. This assumption is consistent with arc experiments [28] which showed that the current to the cathode is conducted through a small area with a diameter of less than a half of centimeter. This is at least twice smaller than the total diameter of the cathode and the arc attachment at the anode.

We assume that the arc covers uniformly the whole anode surface and so the current between the plasma and the anode is conducted through this surface. These arc geometry assumptions imply that the diameter of the arc channel increases from the cathode to the anode (figure 2). For simplicity, we used a 1D formulation of this 2D problem by assuming a prescribed shape of the arc current channel with the current density as

$$J(z) = J_{\text{cathode}} + (J_{\text{anode}} - J_{\text{cathode}}) \times \left(\frac{z}{d}\right)^p \quad (1)$$

where  $d$  is the inter-electrode gap and  $p$  is an exponent. Here, we assumed that the electron current and the ion current follow this form. Most of our calculations were made with  $p = 1$ . In addition, additional calculations were made with  $p = 1/2$  and 2. The results of these calculations showed a low sensitivity of the model to the parameter  $p$ .

Another simplification of our model is that the ablation rate and the arc current were used as external parameters. Moreover, the following experimental arc conditions [2–4] were used for simulations: arc current 65 A, inter-electrode gap 2 mm, anode diameters from 4 to 12 mm. Helium pressure 79 kPa (600 mm Hg). The current density and the plasma temperature at the boundaries between regions I and II, were taken from modeling in [5], namely:  $J = 770 \text{ A cm}^{-2}$  and  $T_e = 0.9 \text{ eV}$ , respectively. Another external parameter of the problem is the carbon density in the inter-electrode gap. It changes as ablation rate changes. Its value should be obtained by solving gas-dynamic equations inside the gap. We performed calculations with this parameter in a very wide range: from 300 Pa to 30 kPa.

The following processes were considered in simulations: (i) electrons are scattered by helium atoms and by carbon ions (Coulomb scattering); (ii) carbon ions collide with helium atoms and electrons. Collisions of carbon ions with carbon atoms and molecules evaporated from the graphite anode creates a drag force that hamper ion flow toward the anode. These collision processes are particularly important for arc operation with a strong anode ablation.

Momentum equations for ions and electrons are

$$-\nabla p_i + R_{i,a} + R_{i,e} + R_{i,He} + enE = 0 \quad (2)$$

$$-\nabla p_e + R_{e,a} + R_{e,i} + R_{e,He} - enE = 0 \quad (3)$$

were  $R_{\alpha,\beta} = \frac{m_\alpha m_\beta}{m_\alpha + m_\beta} n_\alpha n_\beta \bar{v}_{\alpha,\beta} S_{\alpha,\beta} (V_\beta - V_\alpha)$ , Here  $\alpha = i, e, a$ , He.  $S_{\alpha,\beta}$  is the  $\alpha$ - $\beta$  collision cross section,  $m_\alpha$  is mass of the  $\alpha$  particles,  $n_\alpha$  is their density, and  $\bar{v}_{\alpha,\beta}$  is the average relative thermal velocity of the colliding particles.  $V_\alpha$  is the directional velocity of the particles of the  $\alpha$  sort. After introducing  $g_\alpha = n_\alpha V_\alpha$  flux density and excluding the electric field from equations (2) and (3), we have for the ion flux density

$$g_i = -D \nabla n - Ag_e + Bng \quad (4)$$

Here  $g$  is flux density of the evaporated atoms. First two terms in (4) describe diffusion and mutual action of electric field and electron-ion friction. The last term is responsible for ion-evaporated atoms friction. In equation (4),  $g_e = J/e > 0$  is the electron flux density. The flux density of the ablating atoms is  $g = 4G/(m_C \pi d_a^2)$ , where  $G$  is the anode ablation rate ( $\text{kg s}^{-1}$ ), and  $d_a$  is the anode diameter. Note that in equation (4),  $g < 0$ . For coefficients  $A$ ,  $B$  and  $D$  we have

$$D = \frac{T_e + T_a}{\bar{v}_a [n_{He} m_{i,He} S_{i,He} + (n_a + n) m_{a,i} S_{a,i}]} \quad (5)$$

$$A = \frac{m \bar{v}_e (n_a S_{e,a} + n_{He} S_{e,He})}{\bar{v}_a [n_{He} m_{i,He} S_{i,He} + (n_a + n) m_{a,i} S_{a,i}]} \quad (6)$$

$$B = \frac{m_{a,i} S_{a,i}}{n_{He} m_{i,He} S_{i,He} + (n_a + n) m_{a,i} S_{a,i}} \quad (7)$$

The electron density satisfies the continuity equation. In the steady state

$$-\text{div} g_i + \dot{g}_i = 0 \quad (8)$$

where  $\dot{g}_i$  is the ionization-recombination rate. Electric field doesn't appear in equation (8) explicitly. It could be found from the Ohm's generalized (including diffusion) law:

$$J = eg_e = \sigma \left( E + \frac{T_e}{n} \frac{dn}{dz} \right) \quad (9)$$

Discretization of equation (8) for numerical computations in finite difference is shown in the appendix. A forty nodes mesh has been used.

For the source term in equation (8) we wrote:

$$\dot{g}_i = \beta(T_e) n \times [n_S^2(T_e) - n^2] \quad (10)$$

where  $n_S(T_e)$  is the equilibrium (according to the Saha formula) electron density and  $\beta$  is the coefficient of the three-body recombination. The total density of the carbon particles was calculated as corresponding to the chosen ablating rate (independent parameter in our model),  $g \sqrt{\frac{m_C}{2T_a}}$ . Thus, no ionization/recombination equilibrium was considered in the model for the entire arc discharge. Equation (10) describes the deviation from the equilibrium.

For electron temperature we have the following two equations:

$$q = -\kappa \frac{dT_e}{dz} + 2.5 J T_e \quad (11)$$

$$\begin{aligned} \text{div}(q) &= \frac{1}{S} \frac{d}{dz} (S q) \\ &= J E - E_{ion} \dot{g}_i - \frac{3m}{M} n \times n_{He} \bar{v}_e S_{e,He} (T_e - T_a) = 0 \end{aligned} \quad (12)$$

First term in equation (11) describes the heat flux density due to thermal conduction, second—flux of kinetic energy the electrons.  $T_a$ , the temperature of the heavy particles (carbon atoms and ions) and equal to it temperature of the helium atoms were considered as given at some low level and independent on arc characteristics<sup>3</sup>. Equations (11) and (12) can be converted into one equation of the second order, which was re-written in finite differences the same way as equation (8) (see in appendix).

### 3.3. Boundary conditions

The above equations are equally applicable for positive and for negative anode sheath regimes. The difference between these regimes is in the boundary conditions that are set at the plasma-sheath boundary.

**3.3.1. Negative anode sheath.** Negative anode sheath voltage repels electrons which are trapped in the near-anode region. The electron current density obeys the Boltzmann condition:

$$J_e = \frac{en \bar{v}_e}{4} \exp\left(\frac{\Delta V}{kT_e}\right) \quad (13)$$

From an electron kinetic standpoint, electrons cloud in the near-anode region loses its energy due to loss of fast electrons escaping to the anode. In a steady state, the energy necessary to compensate this loss is supplied by the electron thermal conduction:

$$-\kappa_e \nabla T_e = J_e |\Delta V| \quad (14)$$

As for electron density at the plasma-sheath boundary, since the sheath thickness is much narrower than the ion mean free path, the sheath is collisionless: Typical sheath thickness  $\sim 10^{-4}$  cm, whereas the ion free path (ion colliding with helium atoms) is about  $10^{-3}$  cm. Therefore, the ion velocity at the sheath boundary satisfies the Bohm's criterion:

$$J_i = en \sqrt{\frac{kT_e}{M}} \quad (15)$$

**3.3.2. Positive anode sheath.** For the anode sheath with the positive voltage, electrons flow freely to the anode:

<sup>3</sup> Assumption that helium temperature remains the same throughout the gap doesn't mean that the helium atoms do not gain energy in collisions with electrons. The amount of this energy is calculated, see (12). It means that the helium atoms can bring the obtained energy to electrodes without significant temperature change.

$$J_e = en\bar{v}_e \quad (16)$$

According to equation (11), the heat flux density at the plasma-sheath boundary is  $q = -\kappa \frac{dT_e}{dz} + 2.5JT_e$ . At the same time, this heat flux density should be equal to the heat flux density of the freely moving electrons. Assuming a half-Maxwellian electron energy distribution function in the near anode region, the heat flux density is  $\sim 2.5JT_e$ . Comparing these two heat flux density expressions, we find:

$$\nabla T_e = 0 \quad (17)$$

**3.3.3. Consistency of the plasma parameters with the boundary conditions.** We assume that there is no double layer in the near-anode plasma. Therefore, the boundary conditions should be consistent with the plasma parameters at the plasma-sheath boundary. Namely, the electric field at the boundary should be positive in the case of the positive sheath voltage and vice versa. In order to determine, which sheath case is realized, the following procedure was applied for arc simulations:

1. Assuming a sign of the sheath electric field (negative or positive) and setting the corresponding boundary conditions, equations (9)–(12) were solved.
2. The sign of the electric field at the anode sheath boundary with the plasma was obtained and compared to the initial sign of the sheath electric field. If they match, the solution is obtained. If the signs do not match, the opposite sign of the sheath electric field was assumed and steps 1–2 of the procedure were repeated.
3. If neither sign of the sheath voltage provides the match, no solution with the selected parameters was considered.
4. No multiple solutions (both modes at the same set of external parameters) were found.

### 3.4. Parameters used in calculations

We used the following parameters in our calculations.  $S_{i,a}$ , cross section of the resonance charge exchange  $C^+-C$ , was taken from the [29]:  $S_{i,a} = 5 \times 10^{-15} \text{ cm}^2$ . For electron–helium collisions  $S_{e,He} = 2 \times 10^{-16} \text{ cm}^2$  [30]. For electron-carbon atoms collisions, we used  $S_{e,a} = 1 \times 10^{-16} \text{ cm}^2$ . We did not find in literature experimental value for charge exchange collisions  $C^+-He$ . Theoretical values of collisional cross sections for this type of collisions obtained by different authors are scattered [31]. We used the  $S_{i,He} = 2 \times 10^{-15} \text{ cm}^2$  value.

Coefficient of the three-body recombination was calculated according to [32]. Transport properties of the electron gas, including electrical and thermal conductivities, were calculated according to Spitzer–Harm. Scattering of electrons on neutral helium atoms was also taken into account in these calculations.

For parameters at the cathode edge of the discharge, the plasma parameters from [5 and 8] were used:  $J_{\text{cathode}} = 770 \text{ A cm}^{-2}$ ,  $T_{\text{ecathode}} = 0.9 \text{ eV}$ , helium gas pressure is 600 mm Hg, The inter-electrode gap of 2 mm was taken from experiments of [2–4].

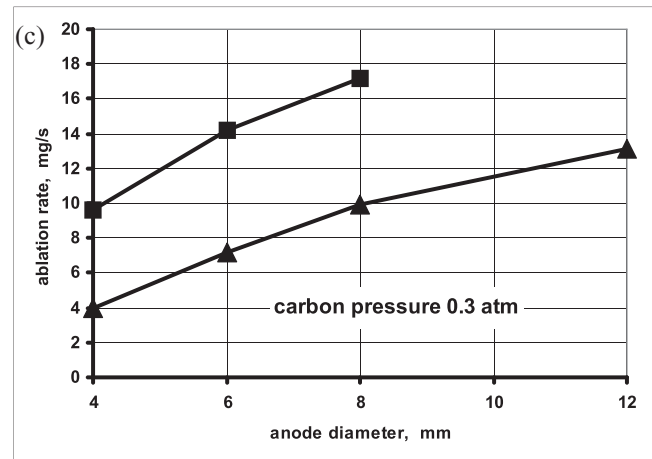
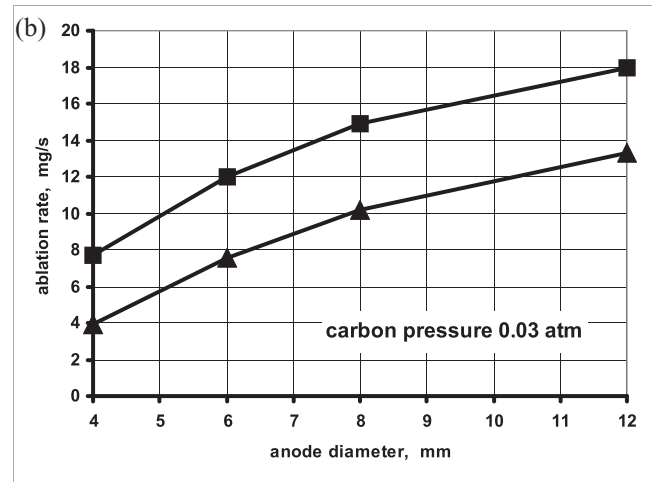
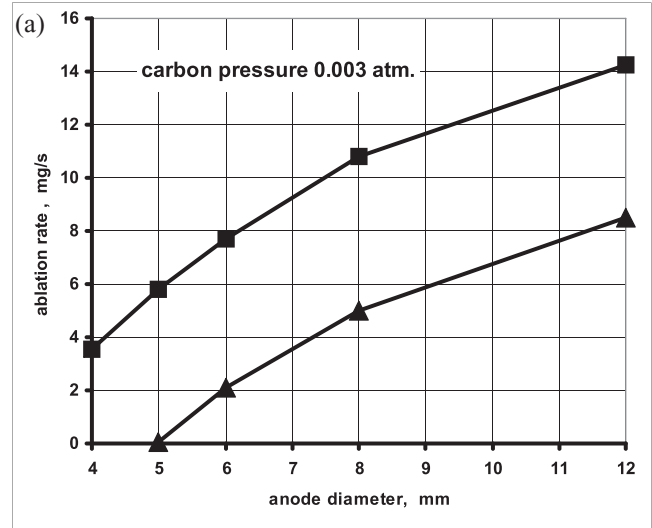


**Figure 3.** Negative anode voltage domain is below the line with triangles (regime I). Positive anode voltage domain is above the line with squares (regime II). (a) Carbon pressure 0.003 atm. (b) Carbon pressure 0.03 atm. (c) Carbon pressure 0.3 atm.

## 4. Results

Distributions of the electron density, electron temperature, and the electric field in the arc plasma were calculated. It was found that both anode sheath regimes, with positive anode voltage

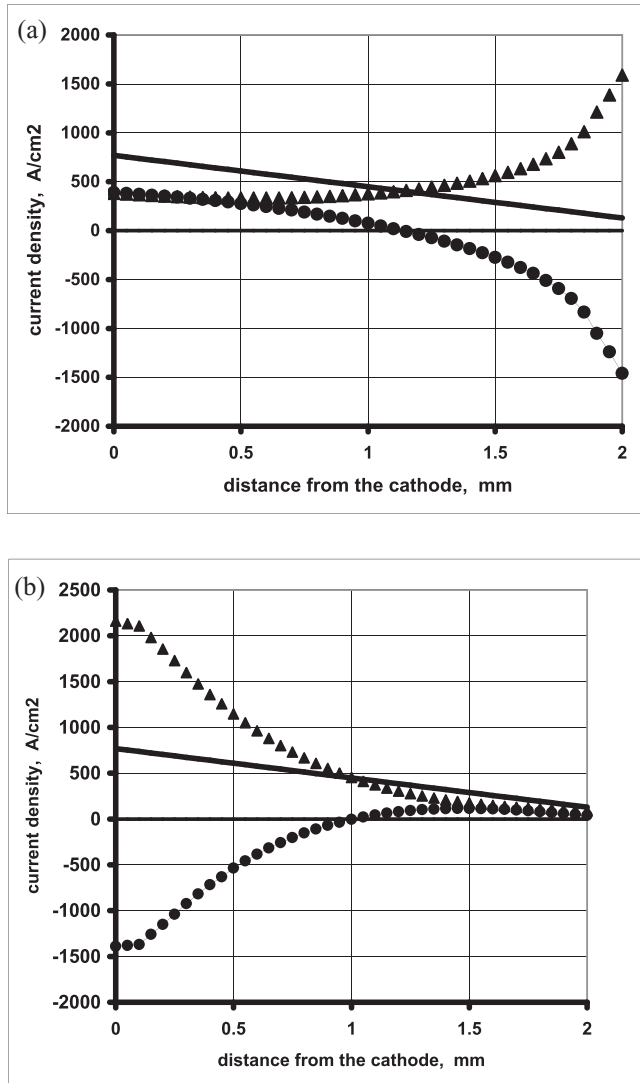


**Figure 4.** (a) Ablation rate 2 mg s<sup>-1</sup>. Circles: Ohmic current density ( $\sigma E$ ), Triangles: diffusion current density  $\sigma \frac{T}{n} \frac{dn}{dz}$ . Solid line: total current density. (b) Ablation rate 16 mg s<sup>-1</sup>. Circles: ohmic current density ( $\sigma E$ ), Triangles: diffusion current density  $\sigma \frac{T}{n} \frac{dn}{dz}$ . Solid line: total current density.

drop and negative anode voltage drop, can exist. The anode sheath regime is determined by the arc current density at the anode and the ablation rate of the anode material. Figure 3 illustrates the operating domains for these anode sheath regimes, namely, regime I and regime II, for three values of the carbon species densities: 300 Pa, 3 kPa and 30 kPa. With high current density at the anode and high ablation rate, the anode sheath is positive (regime II). This result is explained as follows. When the anode current density is high, the diffusion component of the current is not able to sustain the necessary current density, and the electric field at the plasma-sheath is positive. Another process contributing to the formation of the positive anode sheath is that ions are swept away by a strong flow of the atoms and molecules ablating from the anode. A phenomenological description of this mechanism was first discussed in [7].

For the arc operation with a low ablation rate and low current density at the anode, the sheath is negative (regime I).

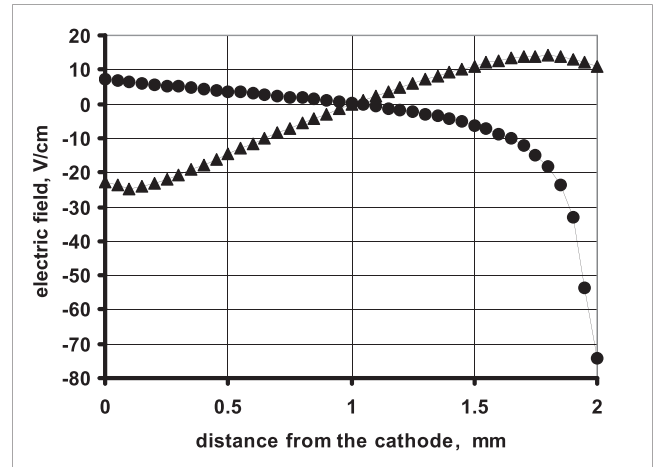


**Figure 5.** Electric field in the inter-electrode space. Circles: ablation rate 2 mg s<sup>-1</sup>. Triangles: ablation rate 16 mg s<sup>-1</sup>.

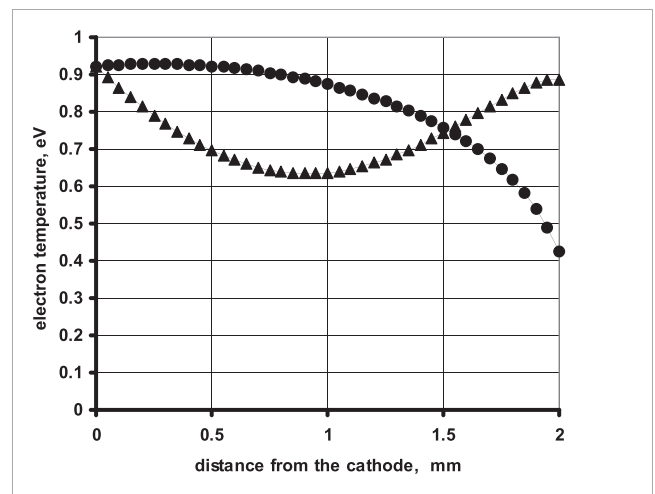


**Figure 6.** Electron temperature in the inter-electrode space. Circles: ablation rate 2 mg s<sup>-1</sup>. Triangles: ablation rate 16 mg s<sup>-1</sup>.

Both anode sheath regimes are shown in figure 3. One can see that for all the carbon pressures, these regimes share no one common boundary. At this moment, it is not clear whether this result is due to the model assumptions or some physical reason. It is possible that the gap corresponds to two different regimes observed experimentally in [2–4]. More accurate modeling including 2D modeling may shed light to this issue.

Below we present result obtained for 3 kPa if not stated otherwise.

#### 4.1. Plasma parameters in the inter-electrode gap

Distributions of the main plasma parameters are different for different anode sheath regimes. In figures 4–8, we compare parameters of the inter-electrode plasma obtained at the same current density at the anode (129 A cm<sup>-2</sup>) but at different ablation rates, 2 mg s<sup>-1</sup> and 16 mg s<sup>-1</sup>. Physically they correspond to the same size but differently cooled anodes that leads to its different ablation rates.

Let us start with parameters of regime I. For this regime, figure 4(a) shows the electron current components driven by

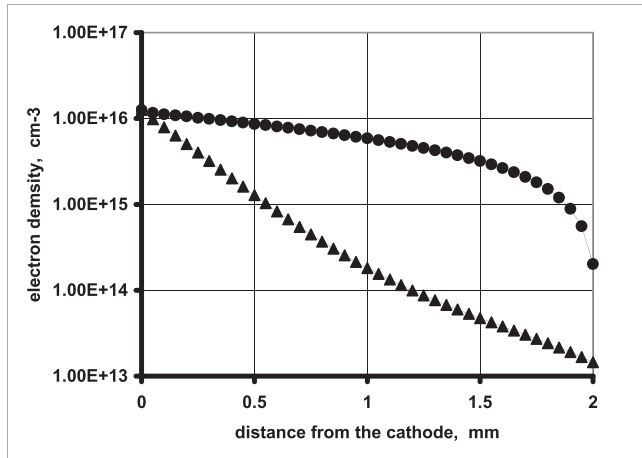


Figure 7. Electron density in the inter-electrode gap. Circles: ablation rate 2 mg s<sup>-1</sup>. Triangles: ablation rate 16 mg s<sup>-1</sup>.

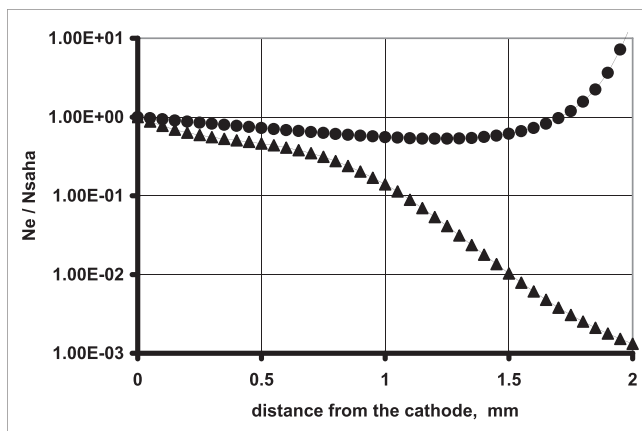


Figure 8. Ratio of electron density to ionization equilibrium density. Circles: ablation rate 2 mg s<sup>-1</sup>. Triangles: ablation rate 16 mg s<sup>-1</sup>.

the Ohmic component  $\sigma E$ , diffusion component  $\sigma \frac{T}{n} \frac{dn}{dz}$ , and the total current density which is sum of these two. Here, the ablation rate is 2 mg s<sup>-1</sup>. As can be seen the diffusion flow near the anode exceeds the total current density. As a result, the electric field reverses and the Ohmic current is directed from the anode to plasma in order to maintain the total current density. Moving in repelling electric field (figure 5), the electrons are cooling down and their temperature decreases toward the anode, figure 6.

Figure 4(b) displays the current components for anode sheath regime II. Here, current density is the same as in the case shown in figure 4, while the ablation rate is 16 mg s<sup>-1</sup>. At the cathode side of the plasma, the diffusion current exceeds the Ohmic one and the electric field in that region repels electrons moving toward the anode (figure 5). Consequently, the electron temperature decreases (figure 6). However, closer to the anode, the ablation of the anode forms the flux of the atoms which sweep the electrons off, causing the electron density to drop in this arc region. The diffusion alone can not sustain the total current to the anode. As a result, the electric field close to the anode becomes positive.

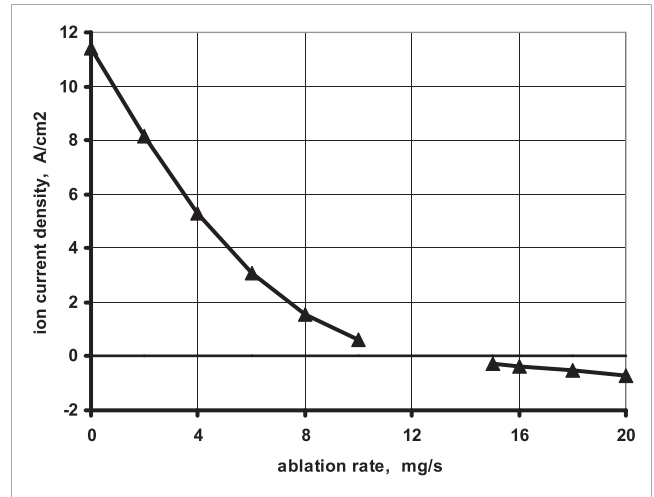


Figure 9. Ion current density at the plasma-sheath boundary.

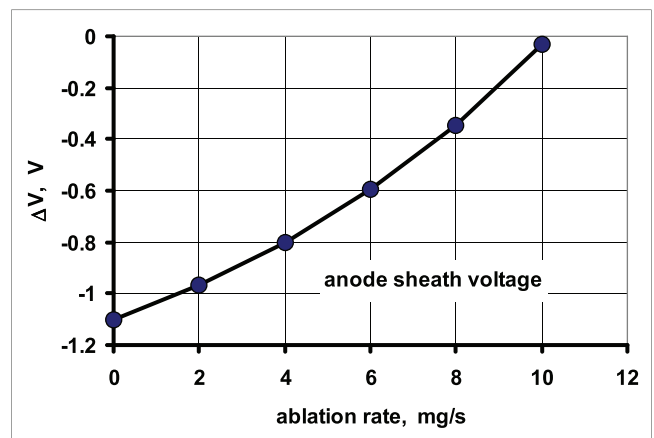


Figure 10. Voltage drop inside the anode sheath. Negative voltage drop regime.

For both anode sheath regimes, figure 7 demonstrates the sweeping effect of the ablation on the electron density distribution. This effect decreases the role of the diffusion and leads to the formation of the positive anode voltage drop.

Note that for both anode sheath regimes, plasma near the anode is not in ionization equilibrium (i.e. the Saha formula is not hold) (figure 8). The reason for high deviation from the ionization equilibrium is that the corresponding ‘ionization length’  $L_{ion} = (D\alpha)^{1/2}$  [10] is comparable or larger than the inter-electrode gap. Here,  $\alpha$  is the ionization rate.

#### 4.2. Arc voltage, ion current and heat flux to the anode

4.2.1. Ion current at the plasma-sheath boundary. The positive and negative anode sheath regimes have different directions of the ion current at the plasma-anode sheath boundary (figure 9). For regime I, ions and electrons are moving in the same direction from plasma to the anode (ion current density is positive). As the ablation rate increases, evaporated atoms push the ions away and the ion current density decreases. Note that simultaneously, the absolute value of the anode voltage drop decreases (figure 10). Finally, for regime II with a high

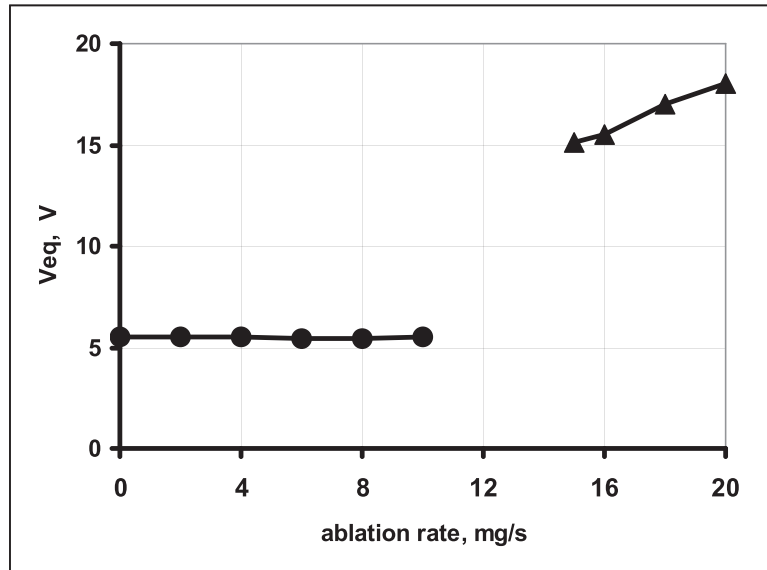


**Figure 11.** Volt equivalent of the anode heat flux. Anode diameter 8 mm. Circles: regime I. Triangles: regime II.

ablation rate the ions move from the anode to the plasma: ion current density changes its sign.

It is important that ions moving from plasma to the anode (regime I) are generated in the plasma, while ions moving from the sheath into plasma (regime II) should be generated inside the anode sheath. The details of this ion generation need a special consideration which is outside the scope of this paper. Here, we restricted the analysis to the following approximate considerations. Electrons entering the positive sheath region should generate less than 0.005 number of ions per electron: ion current density doesn't exceed  $0.7 \text{ A cm}^{-2}$  whereas electron current density at the anode is  $129 \text{ A cm}^{-2}$  (figure 9). When electrons gain enough energy in the positive sheath, they start to ionize atoms and molecules evaporated from the anode (Regime II). Therefore, one might assume the anode voltage drop inside the positive sheath equal to the ionization potential of carbon decreased by the amount of the initial kinetic energy of the electrons entering the sheath.

**4.2.2. Arc voltage.** Once the voltage drop inside the sheath is determined, it is possible to calculate the arc voltage and the heat flux to the anode. The arc voltage was calculated as a sum of the cathode voltage (obtained according to [5]), the voltage in the plasma channel and the anode sheath voltage. The latter two voltages were from the model presented in this work. The result was: 12V for the regime I and 18V for the second regime. Different approximations of the arc channel shapes (parameter  $p$  in formula (1)) result in slight difference in total voltages. For example, in regime I, the difference in voltages between the case  $p = 0.5$  and the case  $p = 2$ , is 0.26V. In regime II, the results are more sensitive to parameter  $p$ .

**4.2.3. Heat flux to the anode.** The heat flux to the anode,  $q_a$ , consists of the heat delivered by electrons, in the form of potential energy (work function  $\phi$ ) and in the form of kinetic energy, and the heat flux density of heavy particles (helium

atoms in our case) brought to the anode by thermal conduction,  $q_{e,\text{He}}$ .

$$q_a = J_e(2.5 T_e + V_{\text{sheath}} + \phi) + q_{e,\text{He}}$$

Note, that term  $J_e V_{\text{sheath}}$  exists in the regime II only. To evaluate the  $q_{e,\text{He}}$ , we calculate the total power transferred from electrons to helium atoms:

$$q_{e,\text{He}} = \int \frac{3m}{M} n \times n_{\text{He}} \bar{v}_e S_{e,\text{He}} (T_e - T_a) dz.$$

Here, we assumed that each electrode receives half of the total power. It is common for arc studies that the energy delivered to the electrodes by heat is expressed in the so-called volt equivalent of the heat that is the heat flux density to current density ratio,  $V_{\text{eq}} = q/J$ . Figure 11 shows that for small anodes with positive anode sheath, the model predict larger voltage equivalent than for large anodes with negative anode sheath. A larger anode heating in regime II explain larger ablation rate measured in this regime as compared to regime I with larger anodes.

## 5. Conclusion

Experiments and model of the arc with ablating anode show two different heating regimes of the anode and correspondingly two different regimes of the anode ablation: (1) very low nearly constant ablation rate and (2) enhanced ablation. The first ablation regime is usually for large anode (in [2–4] for anode diameters  $>6 \text{ mm}$ ) and low current densities, while the second regime is for small anodes (in [2–4] for anode diameters  $<6 \text{ mm}$ ). For two regimes, the calculated domains correspond to these experimental observations. Model attributes these differences to differences in the near-anode processes and the anode sheath. For low ablation regime, the model predicts an ion attractive negative anode sheath, while for high ablation rate, the predicted sheath is electron attractive, positive. For the arc with a positive anode sheath, the

heat flux to the anode is much larger than for the arc with the negative anode sheath. The latter is consistent with the high ablation rate measured for the arcs with small anodes.

In both anode sheath regimes, the diffusion plays significant or even dominant role in conducting the current to the anode. Furthermore, for negative sheath, the diffusion results in fluxes larger than the total current to the anode. As a result, the electric field changes its sign close to anode in order to provide the necessary current density at the anode.

Simulation showed that close to anode and in some in the whole gap, there is no ionization equilibrium. Electron density does not follow the Saha formula.

Among practical implications of these results, the high ablation mode with a positive anode sheath can produce a large feedstock of carbon species for synthesis of nanomaterials. Moreover, the prediction of the anode sheath transition may be applicable for other anodic arc applications, including synthesis of other than carbon nanomaterials and welding arcs.

There are several limitations of the present arc model, including, but not limited to its 1D description. Assuming the near-cathode layer completely autonomous (independent of the plasma in the inter-electrode gap) is another approximation. Moreover, throughout this work only carbon atoms and ions were considered, while it is known that at high temperatures graphite evaporation produces also produce C<sub>2</sub> and C<sub>3</sub> molecules [33]. In fact, experiments [34] showed substantial amounts of C<sub>2</sub> molecules in the arc discharge. However, it is unlikely that the presence of carbon molecules can change the major conclusion of this study. The ionization potential of carbon atoms and, for example, C<sub>2</sub> is very close [35]. Moreover, the dissociation of C<sub>2</sub> molecules is unlikely in the sheath because of a relatively high dissociation energy (7.6 eV [35]).

### Acknowledgments

The authors appreciate their fruitful discussions with V Vekselman and I Kaganovich of Princeton Plasma Physics Laboratory, and M Shneider of Princeton University. This work was supported by the U.S. Department of Energy under Contract No DE-AC02-09CH11466.

### Appendix

Equation (8) is convenient to rewrite in the form

$$-\frac{d}{dz}(S(z)g_i) + S(z)\dot{g}_i = 0$$

where  $S(z)$  = arc current/current density( $z$ ) is the arc channel cross-section obtained from (1). In finite differences it becomes:

$$-\frac{S^{(k+1/2)}g_i^{(k+1/2)} - S^{(k-1/2)}g_i^{(k-1/2)}}{\Delta z} + S^{(k)}\dot{g}_i^{(k)} = 0$$

where

$$g_i^{(k+1/2)} = -D^{(k+1/2)}\frac{n^{(k+1)} - n^{(k)}}{\Delta z} - A^{(k+1/2)}\frac{g_e^{(k+1)} + g_e^{(k)}}{2} + B^{(k+1/2)}\frac{n^{(k+1)} + n^{(k)}}{2} \times \frac{g^{(k+1)} + g^{(k)}}{2}$$

$$g_i^{(k-1/2)} = -D^{(k-1/2)}\frac{n^{(k)} - n^{(k-1)}}{\Delta z} - A^{(k-1/2)}\frac{g_e^{(k)} + g_e^{(k-1)}}{2} + B^{(k-1/2)}\frac{n^{(k)} + n^{(k-1)}}{2} \times \frac{g^{(k)} + g^{(k-1)}}{2}$$

and

$$S^{(k+1/2)} = \frac{S^{(k+1)} + S^{(k)}}{2}, \quad S^{(k-1/2)} = \frac{S^{(k)} + S^{(k-1)}}{2}$$

The coefficients  $A$ ,  $B$  and  $D$  were calculated similarly. In equation (8) written in above form, conservations of the total current and the total flux of the carbon particles are taken in the most straightforward way.

### References

- [1] Iijima S 1991 Helical microtubules of graphitic carbon *Nature* **354** 56
- [2] Fetterman A, Raitses Y and Keidar M 2008 Enhanced ablation of small anodes in a carbon nanotube arc plasma *Carbon* **46** 1322–6
- [3] Ng J, Raitses Y 2014 Role of the cathode deposit in the carbon arc for the synthesis of nanomaterials *Carbon* **77** 80–8
- [4] Ng J and Raitses Y 2015 Self-organized process in the carbon arc for nanosynthesis *J. Appl. Phys.* **117** 063303
- [5] Nemchinsky V and Raitses Y 2015 Atmospheric pressure arc discharge with ablating graphite anode *J. Phys. D.: Appl. Phys.* **48** 245202
- [6] Finkelburg W and Maecker H 1956 *Handbook of Physics* vol 22, ed S Flugge (Berlin: Springer) pp 254–444
- [7] Finkelburg W 1948 The high current carbon arc and its mechanism *J. Appl. Phys.* **20** 468–74
- [8] Bykhovsky D G, Korobova I L, Nemchinsky V A and Peretts L N 1975 Thermal conditions in the anode of the DC welding arc with the electrode positive *Autom. Welding* **28** 7–10
- [9] Panevin I G, Nazarenko I P and Ershov A V 1977 Exploration of the near-anode processes in a high-pressure high-current discharges *Experimental Research of Plasmatrons* ed M F Zhukov (Novosibirsk: Nauka) (in Russian)  
Nazarenko I P and Panevin I G 1989 Analysis of the near-anode processes in argon arc discharge of high pressure *Control Plasma Phys.* **29** 251–61
- [10] Nemchinsky V A and Peretts L N 1977 Anode sheath in a high-pressure, high-current arc *Sov. Phys.—Tech. Phys.* **22** 1083–7
- [11] Dinulescu H A and Pfender E 1980 Analysis of the anode boundary layer of high intensity arcs *J. Appl. Phys.* **51** 3149–57
- [12] Morrow R and Lowke J J 1993 A 1D theory for the electrode sheaths of electric arcs *J. Phys. D: Appl. Phys.* **28** 634–42
- [13] Amakaway T, Jenista J, Heberlein J and Pfender E 1998 Anode-boundary-layer behaviour in a transferred, high-intensity arc *J. Phys. D: Appl. Phys.* **31** 2826–34
- [14] Tanaka M, Ushio M and Wu C S 1999 1D analysis of the anode boundary layer in free-burning argon arcs *J. Phys. D: Appl. Phys.* **32** 605–11

- [15] Yang G and Heberlein J 2006 Anode attachment modes and their formation in a high intensity argon arc *Plasma Sources Sci. Technol.* **16** 529–42
- [16] Dyuzhev G A, Mitrofanov N K, Shkolnik S M and Yur'ev V G 1979 Anode region of high current arc discharge *J. Phys. Colloq.* **40** (suppl. 7) C7-463
- [17] Sanders N A and Pfender E 1984 Measurements of anode falls and anode heat transfer in atmospheric pressure high intensity arcs *J. Appl. Phys.* **55** 714–22
- [18] Leveroni E and Pfender E 1989 Experimental investigation of the anode boundary layer in free-burning arcs *Proc. 9th Symp. on Plasma Chemistry (Pugnochiuso Italy, 4–8 September 1989)*
- [19] Tanaka M and Ushio M 1999 Observations of the anode boundary layer in free-burning argon arcs *J. Phys. D: Appl. Phys.* **32** 906–12
- [20] Heberlein J, Mentel J and Pfender E 2010 The anode region of electric arcs: a survey *J. Phys. D: Appl. Phys.* **43** 023001
- [21] Shkolnik S 2011 Anode phenomena in arc discharges: a review *Plasma Sources Sci. Technol.* **20** 013001
- [22] McKelliget J W and Szekeley J 1983 A mathematical model of the cathode region of a high intensity carbon arc *J. Phys. D: Appl. Phys.* **16** 1007–22
- [23] Bilodeau J-F, Pousse J and Gleizes A 1998 A mathematical model of the carbon arc reactor for fullerene synthesis *Plasma Chem. Plasma Process.* **18** 285–303
- [24] Hinkov I, Farhat S and Scott C D 2005 Influence of the gas pressure on single-wall carbon nanotube formation *Carbon* **43** 2453–62
- [25] Kundrapu M and Keidar M 2012 Numerical simulation of carbon arc discharge for nanoparticle synthesis *Phys. Plasmas* **19** 073510
- [26] Alekseyev N I and Dyuzhev G A 2001 Arc discharge with a vaporizable anode: why is the fullerene formation process affected by the kind of buffer gas? *Techn. Phys.* **46** 1247–55
- [27] Keidar M and Beilis I I 2009 Modeling of atmospheric-pressure anodic carbon arc producing carbon nanotubes *J. Appl. Phys.* **106** 103304
- [28] Yeh Y-W and Raitses Y 2015 Correlation of plasma and material processes in the arc discharge for nano synthesis, submitted to *Carbon*
- [29] Smirnov B M 1985 *Physics of a Weekly Ionized Plasma with Problems and Solutions* (Moscow: Hauka) (in Russian)
- [30] Brown S 1994 *Basic Data of Plasma Physics* (New York: AIP Press)
- [31] Jan-Bo L, Yang W and Ya-Jun Z 2007 Elastic cross section for electron-carbon scattering *Chin. Phys.* **16** 72–6
- [32] Annoloro J, Morel V, Bultel A and Omary P 2012 Global rate coefficients for ionization and recombination of carbon, nitrogen, oxygen, and argon *Phys. Plasmas* **19** 073515
- [33] Pierson H O 1994 *Handbook of Carbon, Graphite, Diamond and Fullerenes. Properties, Processing and Applications* (Park Ridge, NJ: Noyes)
- [34] Lange H, Saidane K, Razafinimanana M and Gleizes A 1999 Temperatures and C<sub>2</sub> column densities in a carbon arc plasma *J. Phys. D: Appl. Phys.* **32** 1024–30
- [35] Diaz-Tendero S, Sanchez G, Hervieux P-A, Alcamí M and Martín F 2006 Ionization potentials, dissociation energies and statistical fragmentation of neutral and positively charged small carbon clusters *Braz. J. Phys.* **36** 529–33